ACS APPLIED MATERIALS & INTERFACES

Research Article

www.acsami.org

Engineered Si Sandwich Electrode: Si Nanoparticles/Graphite Sheet Hybrid on Ni Foam for Next-Generation High-Performance Lithium-Ion Batteries

Chunhui Gao,[†] Hailei Zhao,*[,†,‡] Pengpeng Lv,[†] Tianhou Zhang,[†,‡] Qing Xia,[†] and Jie Wang[†]

[†]School of Materials Science and Engineering, University of Science and Technology Beijing, Beijing 100083, China

[‡]Beijing Key Lab of New Energy Materials and Technologies, Beijing 100083, China

Supporting Information

ABSTRACT: Si-based electrodes for lithium ion batteries typically exhibit high specific capacity but poor cycling performance. A possible strategy to improve the cycling performance is to design a novel electrode nanostructure. Here we report the design and fabrication of Ni/Si-nanoparticles/graphite clothing hybrid electrodes with a sandwich structure. An efficient dip-coating of Si-NPs combined with carbon deposition was adopted to synthesize the unique architecture, where the Si-NPs are sandwiched between the Ni matrix and the graphite clothing. This material architecture offers many critical features that are desirable for high-performance Si-based electrodes, including efficient ion diffusion, high conductivity, and structure durability, thus ensuring the electrode with outstanding electrochemical performance (reversible capacity of 1800 mA h g^{-1} at 2 A g^{-1} after 500 cycles). In addition, the hybrid anode does not require any polymeric binder and conductive additives and holds great potential for application in Li-ion batteries.

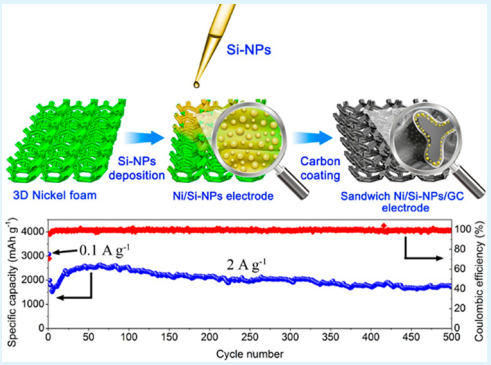

KEYWORDS: *lithium-ion battery, sandwich architecture, Si-based anode, carbon clothing*

1. INTRODUCTION

Lithium-ion batteries continue to find use in a variety of applications and are the ideal choice for the next generation of portable communication devices and hybrid electric vehicles for their merits, including high energy density, low self-discharge rate, and virtually no memory effect.[1] However, the commercially used graphite anode has a limited theoretical capacity of 372 mA h g^{-1}, which is not able to satisfy requirements of advanced batteries. To circumvent the low theoretical specific capacity of graphite, there is significant need to develop new anode materials with high specific capacity.

Silicon anode has attracted much attention because it delivers a capacity nearly ten times higher than that of graphite at room temperature. Theoretically, one silicon atom can maximally react with 4.4 lithium atoms to form a $Li_{4.4}Si$ alloy, reaching a capacity of 4200 mA h g^{-1}.[2] However, the Si anode suffers from a large volume change of ca. 300% upon lithium alloying and dealloying, which causes electrode cracking and pulverization, resulting in a loss of electrical contact between active particles and eventually capacity fading of the electrode. Therefore, extensive efforts have been devoted to solving this problem of Si anode materials. One strategy is to use nanostructured silicon in the form of nanowires, nanorods, nanoscoops, and hollow Si nanospheres to enhance its corresponding cycling stability.[3−6] These nanostructures with free volume can accommodate the strain from Li−Si alloying to ensure the Si-based anodes having better stress tolerance and longer cycle life. The latest design of hierarchical pomegranate structured Si anode, where single silicon nanoparticle was encapsulated by a conductive carbon layer that leaves enough room for expansion and contraction, was capable of charging/discharging for more than 1000 cycles with 97% capacity retention.[7] Another effective strategy, known as nanocompositing, aims to improve the structural stability through employing carbon as the protective coating layer or matrix. The carbon serves three main purposes: (1) the carbon can enhance structural stability and also prevent local capacity fading by maintaining electrical contact between the silicon particles; (2) the carbon can improve the electrical conductivity of Si particles; (3) the carbon can protect the Si particles against direct contact with the electrolyte which may result in the formation of an unstable SEI film. Accordingly, silicon−carbon core−shell nanowires, silicon−graphene nanowires, and silicon−carbon nanotube heteronanostructures have been designed and prepared to improve the structural and electrical integrity of Si anodes.[8−10] In addition, fabricating MSi_x alloys (M═Fe, Ni, Co, Mo, etc.) is another approach to improve the cycling performance while the inactive intermetallic matrices reduce the overall capacity of Si anodes.

The aforementioned works have focused on the issues associated with cycling performance of Si on the nanostructure

Received: October 21, 2014
Accepted: January 5, 2015
Published: January 5, 2015

DOI: 10.1021/am5072755
ACS Appl. Mater. Interfaces 2015, 7, 1693−1698

designing, carbon coating, and Si alloying before the electrode fabrication procedure. In contrast, work on improving the cycling performance of the Si-based anode after the electrode fabrication process has been limited to surface modification of a manufactured electrode with metal-oxide (MO) via atomic layer deposition (ALD).[11] Although ALD-MO coating can reduce the effect of parasitic side reactions between the liquid electrolyte and electrode surface, the coatings are not robust enough to provide structural support when applied to materials such as Si with large volumetric expansion.

The sandwich structure design has advantages in improving the electrochemical performance of the electrode in terms of rate capability and cycle stability, which has been extensively used in anode or cathode materials.[12,13] In this work, in order to overcome the challenge of cycling performance of Si-based anodes, a mechanically robust, flexible graphite clothing (GC) was grown directly on the Ni foam coating with Si nanoparticles (Si-NPs), producing a sandwich Ni/Si-nanoparticles/graphite clothing (Ni/Si-NPs/GC) nanoarchitecture electrode. First, fabrication of a traditional battery electrode usually involves mixing of the active material with conducting carbon and a nonconducting polymeric binder to form a slurry and then casting it onto the current collector followed by drying for several hours.[14] In contrast, our sandwich Ni/Si-NPs/GC electrode was fabricated in two steps and without any postprocessing. Second, an inactive intermetallic phase $NiSi_x$ was produced at the interface of the Ni foam and Si-NPs during the electrodes fabrication process, which can act as a "binder" to weld Si nanoparticles onto the surface of the Ni foam. More importantly, such a design has multiple advantages: (1) the conformal, flexible graphite layer with the electrode that restricts the Si-NPs to fall off from the Ni foam and ensures sufficient electrical conductivity throughout cycling, which improves the cycling stability and rate capability; (2) the 3D Ni foam acted as a conducting network providing efficient electrode conduction and improving mass loading of active materials, which enhanced the energy density; (3) the Si-NPs shorten the transmission way of lithium ions and electrons, which favors the rate performance.

2. EXPERIMENTAL SECTION

2.1. Material Synthesis. The Si suspension was prepared by dispersing the as received silicon powders (crystalline, average particle size ~100 nm, Alfa Aeser) into ethanol with the assistance of ultrasonicaiton. For fabrication of sandwich Ni/Si-NPs/GC electrode, liquid droplets of Si-NPs suspension were dropped on the Ni foam (diameter: 8.0 mm, thickness: 0.50 mm, weight: 14−15 mg, porosity: 98%) to fill the Ni pores. The filled Ni foam was dried under infrared lamp and then placed into a long quartz boat of a horizontal tube furnace for generation of graphite clothing with a chemical vapor deposition process. Toluene is used as the carbon source and is introduced into the reactor by $95\%Ar/5\%H_2$ bubbling at room temperature. The flow rate of $95\%Ar/5\%H_2$ is controlled at 100 SCCM. The reaction temperature is controlled at 800 °C, and the duration is about 20−30 min. To obtain the weight of active materials, the nickel foam was weighed before and after the dip-coating and graphite clothing forming processes. The prepared sandwich Si-NPs/GC electrode consisted of ~80% (weight percentage) Si-NPs and ~20% (weight percentage) carbon, and the total weight of the anode material (Si-NPs/GC) was 0.5−1.5 mg, corresponding to 1.0−3.0 mg/cm^2.

2.2. Materials Characterization. The morphologies of the as-received Ni foam, Si-NPs, and electrode surface were characterized by field emission scanning electron microscopy (FE-SEM, SUPRA55) and transmission electron microscopy (TEM, JEOL 2010). The as-received Si-NPs and sandwich Si-NPs/GC electrode were characterized by powder X-ray diffraction (XRD; Rigaku, D/max-A X-ray diffractometer) with Cu Kα radiation. Raman scattering spectra were recorded on a LabRAM HR Evolution spectrometer to investigate the characteristics of GC and the Si-based multicomponent. X-ray photoelectron spectroscopy (XPS) spectra of samples were obtained using a PHI 5000C ESCA System with monochromatic Mg Kα radiation as X-ray source.

2.3. Electrochemical Test. Coin type half cells were fabricated in an argon-filled glovebox with Li metal as the counter electrode. A polypropylene film (Celgard 2400) was employed to separate the two electrodes, and the 1 M $LiPF_6$ dissolved in a nonaqueous solution of ethylene carbonate (EC), diethyl carbonate (DEC), and dimethyl carbonate (DMC) (1:1:1 by volume) was employed as electrolyte. The charge/discharge tests were carried out at different current densities between 0.01 and 1.5 V vs Li/Li$^+$, using a LAND CT2001A battery test system (Wuhan, China). Cyclic voltammetry (CV) at a scan rate of 0.1 mV s^{-1} between 0.01 and 1.5 V was conducted using Arbin BT-2000 Battery Tester (America).

3. RESULTS AND DISCUSSION

Figure 1 illustrates the preparation procedure of the sandwich Ni/Si-NPs/GC hybrid electrode and the Raman spectra of the

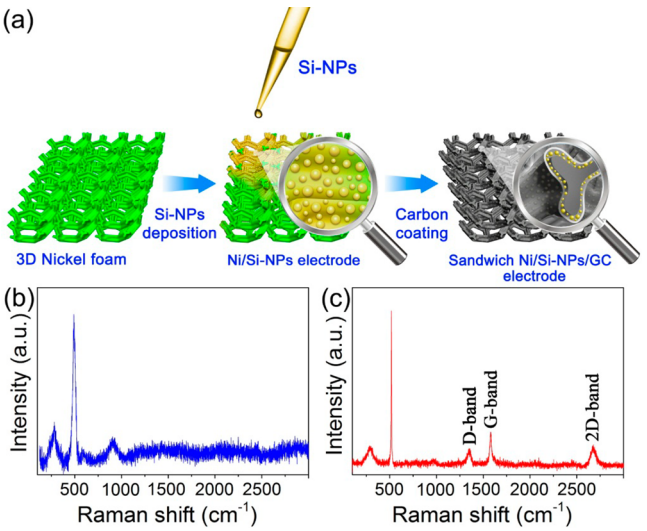

Figure 1. (a) Schematic illustration for preparing sandwich Ni/Si-NPs/GC hybrid electrodes; Raman spectra of the electrode surfaces of Ni/Si-NPs (b) and Ni/Si-NPs/GC (c).

electrode surfaces of Ni/Si-NPs and Ni/Si-NPs/GC. The Ni/Si-NPs/GC electrode has an excellent flexibility, which can be clearly demonstrated in Figure S1 in the Supporting Information (SI). No rupture arising from the tensile stress was observed when the electrode was subjected to bending. This flexibility is attributed to the toughness of Ni foam and a coherent, intact structure of graphite clothing. Raman spectroscopy was used to study the change in chemical structure of Ni/Si-NPs and the Ni/Si-NPs/GC electrodes (Figure 1b,c). As expected, a broad peak centered at 500 cm^{-1} was observed for the Ni/Si-NPs electrode, which corresponds to the lattice vibration of silicon. This broad peak for Ni/Si-NPs/GC electrode sharpens and shifts to slightly higher wave numbers, which is attributed to the ordering of the Si-NPs promoted by the annealing process at 800 °C. In addition, two peaks appear at 283 and 927 cm^{-1}, which is assignable to the Si−O−Si bending and stretching vibrations of silica on the Si-NPs surface.[15] GC was confirmed by the carbon characteristic peaks

DOI: 10.1021/am5072755
ACS Appl. Mater. Interfaces 2015, 7, 1693−1698

of D and G band at 1355 and 1600 cm^{-1}, with an I_D/I_G ratio of 0.70. The shape and position of these peaks are explained by structural disorder and defects within the graphite. The 2D peak at 2675 cm^{-1} (Figure 1c) indicates the formation of multilayer graphene during the GC forming process.[16]

Figure 2a shows the XRD pattern of the sandwich Ni/Si-NPs/GC hybrid electrode along with reference peaks of silicon,

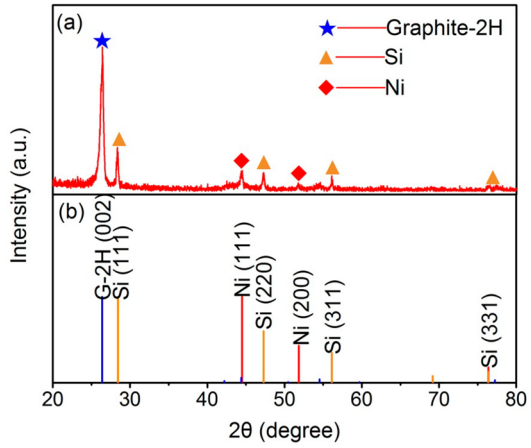

Figure 2. (a) XRD pattern of sandwich Ni/Si-NPs/GC hybrid electrode and (b) reference peaks of silicon (JCPDS 5-0565), Ni (JCPDS 65-2865), and graphite-2H (JCPDF 41-1487).

nickel, and graphite-2H (Figure 2b). The XRD pattern for the as-received Si-NPs is also provided in the SI, Figure S2 . Huang et al. reported that nickel silicide could form at 700 °C.[17] However, it is not shown in the XRD pattern in this work although the Si NP filled Ni foam has been heat-treated at 800 °C, which may be caused by the trace content of nickel silicide. To ascertain the existence of nickel silicide on the interface of Ni foam and Si-NPs, XPS analysis was conducted and the result is shown in the SI, Figure S3. The broad peak over a binding energy range of 850−858 eV corresponds to Ni metal and nickel silicide (SI, Figure S3a; Ni (852.7 eV), NiSi (853.9 eV), and $NiSi_2$ (854.6 eV)). These intermetallic phases can act as binders to prevent Si-NPs from losing electrical contact upon repeated charge/discharge cycles, promoting cycling performance. In addition, XPS analysis of C_{1s} core level spectrum is shown in the SI, Figure S3b. Two peaks can be extracted from the C_{1s} spectrum using Gaussian−Lorentzian simulation. The one appearing at 284.6 eV is the prominent C_{1s} peak of C−C bonds and that locating at 286.6 eV arises from C−O bonds.[18] No peak can be attributed to carbon bonded to Si, indicating the absence of SiC compound.

The morphology of as-received Ni foam and Si-NPs is characterized by FE-SEM and TEM (SI, Figure S4a-c). Typically, the Ni foam consists of a hierarchical 3D macroporous network and the spherical Si-NPs have an average diameter of ∼100 nm. An amorphous SiO_x shell can be observed on the surface of Si-NPs (SI, Figure S4d). With respect to the Ni/Si-NPs, the Si-NPs uniformly dispersed on the network of dendritic Ni microfibers (SI, Figure S4e,f).

Figure 3a shows the FE-SEM image of the resulting electrode with a GC layer covered on the surface of Ni foam. Due to the difference of the thermal expansion coefficients between nickel and graphite, ripples and wrinkles (Figure 3b) were formed on the GC. These ripples and wrinkles can provide an adequate diffusion path during the charging/discharging process. Besides,

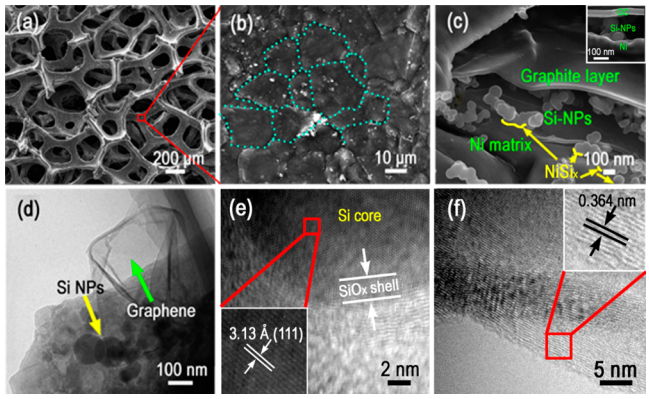

Figure 3. FE-SEM images of the sandwich Ni/Si-NPs/GC hybrid electrode at low (a) and high (b) magnifications. FE-SEM image of the cross-section of the sandwich Ni/Si-NPs/GC hybrid electrode (c) (inset: sandwich structure of Ni/Si-NPs/GC hybrid electrode). TEM images of the sandwich Ni/Si-NPs/GC hybrid electrode (d). HR-TEM images of the edge of Si particle (e) (inset: magnified HR-TEM image of Si particle) and graphene multilayers (f) (inset: magnified HR-TEM image of graphene multilayers).

the cross-section of the electrode with a thickness of ∼50 nm graphite layer covered on the surface of Si-NPs is shown in Figure 3c. There is sufficient void space between the Ni matrix and GC, which can accommodate the large volume change caused by lithiation/delithiation of Si and thus maintain the electrode integrity. A careful observation suggests that some Si-NPs are welded onto the surface of the Ni foam instead of simple physical contact between them. XPS analysis confirms the existence of $NiSi_x$ (SI, Figure S3), which should form on the interface between Ni foam and Si-NPs (marked by yellow lines and arrows in Figure 3c). The $NiSi_x$ can act as a "binder" to weld Si nanoparticles onto the surface of Ni foam to increase the structural stability of the electrode. Furthermore, a much clearer sandwich nanostructure is shown in the inset of Figure 3c, and Si-NPs can be observed to be sandwiched between Ni matrix and GC. In addition to the graphite, TEM observation reveals the existence of graphene-sheets covering the surface of Si-NPs (Figure 3d), which agrees well with the results of Raman spectroscopy. The formation of multilayer graphene sheet is probably promoted by the catalysis of the Ni foam at high tempereature.[19] As shown in Figure 3d, the Si-NPs with clear lattice fringes in core (inset of Figure 3e) is covered by an intermediate amorphous SiO_x shell with a thickness of ∼5 nm and an outer carbon layer. The SiO_x shell could interact with Li^+ forming inactive Li_4SiO_4 and Li_2O phases which are reported to be capable of effectively alleviating Si volume change.[20,21] In addition, the graphene multilayers are further confirmed by HR-TEM observation, as marked by the green arrow in Figure 3d and shown in Figure 3f, which combined with the graphite sheet is favor of electronic conduction. As a result, this unique sandwich nanostructure can not only improve the electronic conductivity of the electrode but also provide void space to accommodate the volume change of Si-NPs during lithiation, maintaining excellent cycling performance in LIB applications.

The electrochemical performance of the sandwich Ni/Si-NPs/GC electrode at a low current density (0.1 A g^{-1}) and a voltage range of 1.5 to 0.01 V is shown in Figure 4a. It shows that the electrode achieves a first cycle efficiency of 71%, and an initial charge capacity of 2900 mA h g^{-1}. This reversible specific

DOI: 10.1021/am5072755
ACS Appl. Mater. Interfaces 2015, 7, 1693−1698

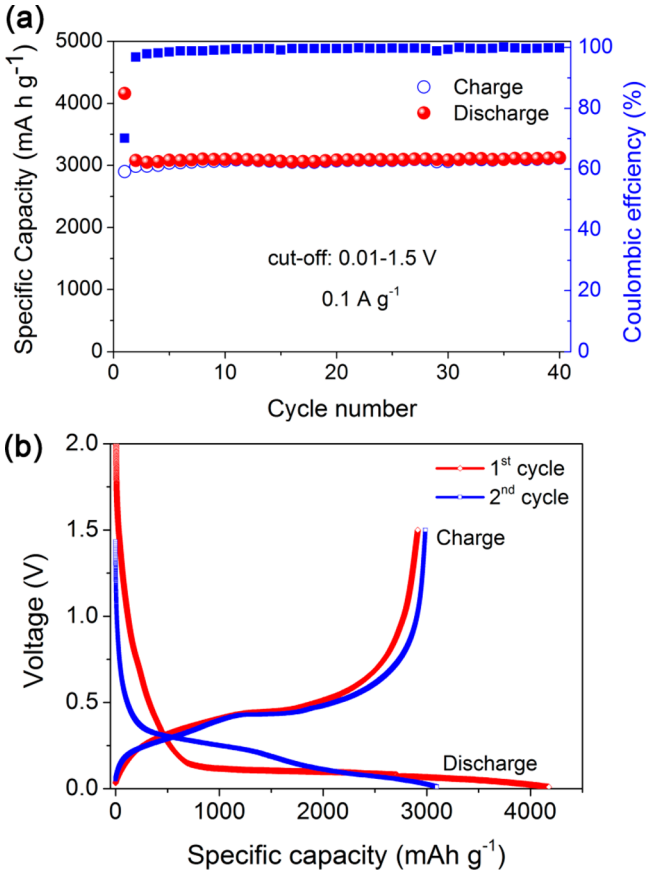

Figure 4. (a) Cycling performance of the sandwich Ni/Si-NPs/GC hybrid electrode at 0.1 A g^{-1} with cut off voltage of 1.5 to 0.01 V; (b) galvanostatic voltage profile at 0.1 A g^{-1}.

capacity of our sandwich Ni/Si-NPs/GC electrode is over eight times higher than that of the theoretical capacity of graphite. The irreversible capacity loss is mainly caused by the solid electrolyte interphase (SEI) formation at ~0.7 V (Figure 4b) and the reaction of oxygen-containing functional groups on the graphite with lithium ions.[22,23] When the current density increases to 2.0 A g^{-1}, the sandwich Ni/Si-NP/GC electrode delivered a capacity of ca. 1900 mA h g^{-1} with approximately 95% capacity retention after 500 cycles (Figure 5a). The capacity fluctuates somewhat between 50 and 500th cycles, which is mainly caused by the ambient temperature change during the test. The cycle stability (0.01% decay per cycle) is rare to obtain to date. Coulombic efficiency is an indicator of the reversibility of the electrode reaction. The pulverization of Si-NPs usually results in SEI rupture and reformation which decreases Coulombic efficiency, especially in later cycles.[8] The average Coulombic efficiency from the 10th to 500th is as high as 99.5%.

To demonstrate the effect of various loadings of Si-NPs/GC on the electrochemical performance of sandwich Ni/Si-NPS/GC electrodes, the electrodes with various loadings of active material were cycled at 100 mA g^{-1} to compare their performances. With increasing loading amount of active material, the mass specific capacity decreases gradually (SI, Figure S5a), which is probably caused by the thickened Si-NPs/GC layer that will cause retarded electrode reaction kinetics. The areal capacity of electrodes with different amounts of active material is calculated and illustrated in the SI, Figure S5b. The areal capacity increases considerably with increasing loading amount of active materials; it can reach ca. 8.0 mA h cm^{-2} for the electrode with 3.12 mg cm^{-2} loading of active material. It is worth noting that a good cycling performance is achieved for all of the investigated three electrodes, suggesting the superiority of the proposed sandwich Ni/Si-NPS/GC electrode structure.

The rate capability of the Ni/Si-NPs/GC electrode at high current density up to 4 A g^{-1} was measured and the result is shown in Figure 5b. The average charge capacities at these rates are 2860, 2750, 2650, 2600, 2270, 2030, and 1500 mA h g^{-1} for 0.1, 0.3, 0.5, 0.8, 1.0, 2.0, and 4.0 A g^{-1}, respectively. These excellent charge capacities well exemplify the high rate capability offered by the sandwich nanostructures. When the rate returned to 0.1 A g^{-1}, the charge capacity recovered to

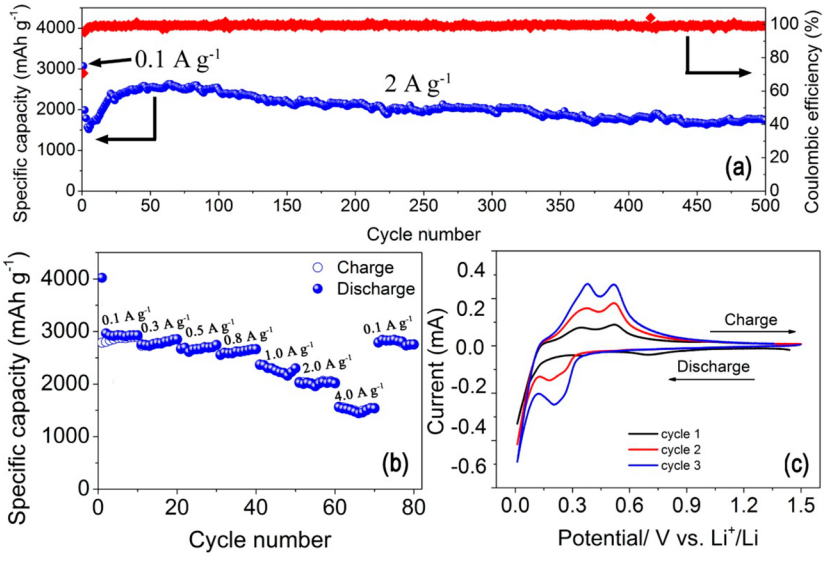

Figure 5. Electrochemical cycling performance of the sandwich Ni/Si-NPs/GC hybrid electrode under charge/discharge cycles from 1.5 to 0.01 V with a charge/discharge current of 2.0 A g^{-1}. (b) Capacity of the Ni/Si-NPs/GC hybrid electrode cycled at various current densities. (c) CV curves of the Ni/Si-NPs/GC hybrid electrode at a scan rate of 0.1 mV s^{-1} over potential window of 0.01−1.5 V versus Li/Li^+.

DOI: 10.1021/am5072755
ACS Appl. Mater. Interfaces 2015, 7, 1693−1698

2790 mA h g^{-1} compared with the 2860 mA h g^{-1} recorded for the initial 0.1 A g^{-1} rate cycle, indicating capacity fading of only 2.4%.

The excellent electrochemical performance of the sandwich Ni/Si-NPs/GC electrode is contributed by several advantages of the unique electrode structure: (1) the $NiSi_x$ phase formed between Ni foam and Si-NPs enhances the electrode stability by welding the active Si particles onto the Ni substrate to prevent its exfoliation from the electrode; (2) the macropores of Ni foam provide sufficient space to accommodate the volume expansion of Si upon lithiation, and more contact area between the active material and the electrolyte solution to promote the electrochemical reaction; (3) the small particle size of Si-NPs (~100 nm) possesses strong resistance to the mechanical failure according to the work by Liu et al.[24] and could offer short distance for lithium ion diffusion, ensuring good cycling stability and high rate capability; (4) the graphite cloth and the trace of graphene multisheet as well as the Ni foam provide a fast electron transport network for electrode reaction.

Figure 5c shows the CV curves of Ni/Si-NPs/GC electrode for the first three cycles. Inspection of the first cycle CV reveals that there are two peaks at 0.7 and 0.10 V in the cathodic branch; the former corresponds to formation of SEI film, while the latter is attributed to the conversion of the Si to the Li_xSi phase. The two peaks at ~0.35 and 0.53 V in the anodic branch correspond to delithiation of the Li_xSi phase to Si.[25] Upon discharge, the lithiation peaks shift positively and are separated into two peaks at 0.1 and 0.23 V due to the formation of various amorphous Li−Si phases.[26] The anode and cathodic peaks increase with cycling due to activation of more material to react with Li in each scan, which is consistent with the finding of others and our results introduced in Figure 5a.[2,27−29]

The morphologies of the sandwich Ni/Si-NPs/GC electrode surface after first and 350th cycles were examined to confirm the excellent cycle durability of the electrode. The FE-SEM image of sandwich Ni/Si-NPs/GC electrode after the first cycle is shown in the SI, Figure S6a. The ripples and wrinkles observed on the electrode surface become smooth after initial cycle, which is most likely ascribed to the formation of SEI film. This is evidenced by the lower Columbic efficiency during the initial cycle (Figure 4b). After the 350th cycle, the surface morphology (SI, Figure S6b) stays almost unchanged, which implies that the unique sandwich structure ensures the excellent cycle durability of the electrode.

Although the prepared sandwich Ni/Si-NPs/GC electrode exhibits excellent electrochemical performance, its lower volumetric energy density caused by the large amount of macropores in Ni foam may prevent it from practical application. This work provides a design strategy for a superior performance electrode with excellent cycling stability and high specific capacity. In future work, by optimizing the pore size and porosity of the Ni foam, the loading of active material could be significantly increased and therefore the volumetric energy density of LIBs can be enhanced.

4. CONCLUSION

In conclusion, the sandwich Ni/Si-NPs/GC hybrid electrode was prepared through a novel and economical process. Such an electrode presents excellent cycling performance as the anode in Li-ion batteries. The sandwich Ni/Si-NPs/GC hybrid electrode with outmost graphite clothing provides a strong structural buffer, high electrical conductivity, which reveals a new approach to solving an old problem of cycling stability, providing a scalable methodology for treating commercial Si-NPs. The simplified process represents a promising avenue for the production of industrially viable high-performance Si-based electrodes, which could be extended for manufacturing of the next-generation Li-ion batteries.

■ ASSOCIATED CONTENT

Supporting Information

Optical micrograph of sandwich Ni/Si-NPs/GC hybrid electrode, XRD pattern of the as-received Si-NPs, XPS spectrum of sandwich Ni/Si-NPs/GC hybrid electrode, FE-SEM images of the as-received Ni foam, Si-NPs and Ni foam covered with Si-NPs, TEM images of the as-received Si-NPs, different reversible capacities and areal capacities of the sandwich Ni/Si-NPs/GC electrodes with various active material loadings, and FE-SEM images of electrodes after 1st and 350th cycles. This material is available free of charge via the Internet at http://pubs.acs.org.

■ AUTHOR INFORMATION

Corresponding Author

*E-mail: hlzhao@ustb.edu.cn. Phone: (+86) 10 82376837. Fax: (+86) 10 82376837.

Notes

The authors declare no competing financial interest.

■ ACKNOWLEDGMENTS

This work was financially supported by National Basic Research Program of China (2013CB934003), "863"program (2013AA050902), National Nature Science Foundation of China (21273019), Guangdong Industry-Academy-Research Alliance (2013C2FC0015), the Program of Introducing Talents of Discipline to Universities (B14003) and Science and Technology Plan Project of Tangshan City (14130278a).

■ REFERENCES

(1) Yaser, A. L.; Davidson, I. *Nanotechnology for Lithium-Ion Batteries*; Springer: New York, 2012; Vol. 3, p 43.

(2) Chan, C. K.; Peng, H.; Liu, G.; Mcilwrath, K.; Zhang, X. F.; Huggins, R. A.; Cui, Y. High-Performance Lithium Battery Anodes Using Silicon Nanowires. *Nat. Nanotechnol.* **2008**, *3*, 31−35.

(3) Kim, H.; Cho, J. Superior Lithium Electroactive Mesoporous Si@Carbon Core-Shell Nanowires for Lithium Battery Anode Material. *Nano Lett.* **2008**, *8*, 3688−3691.

(4) Au, M.; He, Y.; Zhao, Y.; Ghassemi, H.; Yassar, R. S.; Garcia-Diaz, B.; Adams, T. Silicon and Silicon-Copper Composite Nanorods for Anodes of Li-Ion Rechargeable Batteries. *J. Power Sources* **2011**, *196*, 9640−9647.

(5) Krishnan, R.; Lu, T. M.; Koratkar, N. Functionally Strain-Graded Nanoscoops for High Power Li-Ion Battery Anodes. *Nano Lett.* **2010**, *11*, 377−384.

(6) Yao, Y.; McDowell, M. T.; Ryu, I.; Wu, H.; Liu, N.; Hu, L.; Nix, W. D.; Cui, Y. Interconnected Silicon Hollow Nanospheres for Lithium-Ion Battery Anodes with Long Cycle Life. *Nano Lett.* **2011**, *11*, 2949−2954.

(7) Liu, N.; Lu, Z.; Zhao, J.; McDowell, M. T.; Lee, H. W.; Zhao, W.; Cui, Y. A Pomegranate-Inspired Nanoscale Design for Large-Volume-Change Lithium Battery Anodes. *Nat. Nanotechnol.* **2014**, *9*, 187−192.

(8) Cui, L. F.; Yang, Y.; Hsu, C. M.; Cui, Y. Carbon-silicon Core-Shell Nanowires as High Capacity Electrode for Lithium Ion Batteries. *Nano Lett.* **2009**, *9*, 3370−3374.

(9) Xu, W.; Flake, J. C. Composite Silicon Nanowire Anodes for Secondary Lithium-Ion Cells. *J. Electrochem. Soc.* **2010**, *157*, A41−A45.

DOI: 10.1021/am5072755
ACS Appl. Mater. Interfaces 2015, 7, 1693−1698

(10) Wang, W.; Kumta, P. N. Nanostructured Hybrid Silicon/Carbon Nanotube Heterostructures: Reversible High-Capacity Lithium-Ion Anodes. *ACS Nano* **2010**, *4*, 2233−2241.
(11) Piper, D. M.; Travis, J. J.; Young, M.; Son, S. B.; Kim, S. C.; Oh, K. H.; George, S. M.; Lee, S. H. Reversible High-Capacity Si Nanocomposite Anodes for Lithium-Ion Batteries Enabled by Molecular Layer Deposition. *Adv. Mater.* **2014**, *26*, 1596−1601.
(12) Guo, X.; Fan, Q.; Liang, J.; Ji, W.; Peng, L.; Guo, X.; Ding, W.; Chen, Y. Sandwich-like $LiFePO_4$/Graphene Hybrid Nanosheets: in situ Catalytic Graphitization and Their High-Rate Performance for Lithium Ion Batteries. *J. Mater. Chem. A* **2013**, *1*, 11534−11538.
(13) Liu, J.; Chen, J.; Wei, X.; Lou, X.; Liu, X. Sandwich-Like, Stacked Ultrathin Titanate Nanosheets for Ultrafast Lithium Storage. *Adv. Mater.* **2011**, *23*, 998−1002.
(14) Chan, C. K.; Zhang, F.; Cui, Y. High Capacity Li Ion Battery Anodes Using Ge Nanowires. *Nano Lett.* **2008**, *8*, 307−309.
(15) Kingma, K.; Hemley, R. Raman Spectroscopic Study of Microcrystalline Silica. *Am. Mineral.* **1994**, *79*, 269−273.
(16) Ferrari, A. C.; Meyer, J. C.; Scardaci, V.; Casiraghi, C.; Lazzeri, M.; Mauri, F.; Piscanec, S.; Jiang, D.; Novoselov, K. S.; Roth, S.; Geim, A. K. Raman Spectrum of Graphene and Graphene Layers. *Phys. Rev. Lett.* **2006**, *97*, 187401.
(17) Huang, X.; Pu, H.; Chang, J.; Cui, S.; Hallac, P. B.; Jiang, J.; Hurley, P. T.; Chen, J. Improved Cyclic Performance of Si Anodes for Lithium-Ion Batteries by Forming Intermetallic Interphases Between Si Nanoparticles and Metal Microparticles. *ACS Appl. Mater. Interfaces* **2013**, *5*, 11965−11970.
(18) Wu, K. Y.; Chen, W. Y.; Hwang, J.; Wei, K. K.; Kou, C. S.; Lee, C. Y.; Liu, Y. L.; Huang, H. Y. Structure Modification of Highly Ordered Pyrolytic Graphite by Ar Plasma Beam Scanning at Different Incident Angles. *Appl. Phys. A: Mater. Sci. Process.* **2009**, *95*, 707−712.
(19) Losurdo, M.; Giangregorio, M. M.; Capezzuto, P.; Bruno, G. Graphene CVD Growth on Copper and Nickel: Role of Hydrogen in Kinetics and Structure. *Phys. Chem. Chem. Phys.* **2011**, *13*, 20836−20843.
(20) Lee, J. I.; Choi, N. S.; Park, S. Highly Stable Si-based Multicomponent Anodes for Practical Use in Lithium-Ion Batteries. *Energy Environ. Sci.* **2012**, *5*, 7878−7882.
(21) Jeong, G.; Kim, J. H.; Kim, Y. U.; Kim, Y. J. Multifunctional TiO_2 Coating for a SiO Anode in Li-Ion Batteries. *J. Mater. Chem.* **2012**, *22*, 7999−8004.
(22) Yin, S. Y.; Zhang, Y. Y.; Kong, J. H.; Zou, C. J.; Li, C. M.; Lu, X. H.; Ma, J.; Boey, F. Y. C.; Chen, X. D. Assembly of Graphene Sheets into Hierarchical Structures for High-Performance Energy Storage. *ACS Nano* **2011**, *5*, 3831−3838.
(23) Wu, Z. S.; Ren, W. C.; Wen, L.; Gao, L. B.; Zhao, J. P.; Chen, Z. P.; Zhou, G. M.; Li, F.; Cheng, H. M. Graphene Anchored with Co_3O_4 Nanoparticles as Anode of Lithium Ion Batteries with Enhanced Reversible Capacity and Cyclic Performance. *ACS Nano* **2010**, *4*, 3187−3194.
(24) Liu, X. H.; Zhong, L.; Huang, S.; Mao, S. X.; Zhu, T.; Huang, J. Size-Dependent Fracture of Silicon Nanoparticles During Lithiation. *ACS Nano* **2012**, *6*, 1522−1531.
(25) Hassan, F. M.; Chabot, V.; Elsaued, A. R.; Xiao, X.; Chen, Z. Engineered Si Electrode Nanoarchitecture: A Scalable Postfabrication Treatment for the Production of Next-Generation Li-Ion Batteries. *Nano Lett.* **2014**, *14*, 277−283.
(26) Pollak, E.; Salitra, G.; Baranchugov, V.; Aurbach, D. In situ Conductivity, Impedance Spectroscopy, and ex situ Raman Spectra of Amorphous Silicon during the Insertion/Extraction of Lithium. *J. Phys. Chem. C* **2007**, *111*, 11437−11444.
(27) Ge, M.; Rong, J.; Fang, X.; Zhou, C. Porous Doped Silicon Nanowires for Lithium Ion Battery Anode with Long Cycle Life. *Nano Lett.* **2012**, *12*, 2318−2323.
(28) Li, J.; Dahn, J. R. An in situ X-ray Diffraction Study of the Reaction of Li with Crystalline Si. *J. Electrochem. Soc.* **2007**, *154*, A156−A161.
(29) Chen, X.; Li, X.; Ding, F.; Xu, W.; Xiao, J.; Cao, Y.; Meduri, P.; Liu, J.; Graff, G. L.; Zhang, J.-G. Conductive Rigid Skeleton Supported Silicon as High-Performance Li-Ion Battery Anodes. *Nano Lett.* **2012**, *12*, 4124−4130.

DOI: 10.1021/am5072755
ACS Appl. Mater. Interfaces 2015, 7, 1693−1698